THE JOURNAL OF PHYSICAL CHEMISTRY LETTERS
A JOURNAL OF THE AMERICAN CHEMICAL SOCIETY

pubs.acs.org/JPCL

Letter

A "Steady-State" Relaxation Dispersion Nuclear Magnetic Resonance Experiment for Studies of Chemical Exchange in Degenerate ^{1}H Transitions of Methyl Groups

Vitali Tugarinov,* Yusuke Okuno, Francesco Torricella, Theodoros K. Karamanos, and G. Marius Clore*

Cite This: *J. Phys. Chem. Lett.* 2022, 13, 11271−11279

Read Online

ACCESS | Metrics & More | Article Recommendations | Supporting Information

ABSTRACT: Degenerate spin-systems consisting of magnetically equivalent nuclear spins, such as a $^{1}H_3$ spin-system in selectively $^{13}CH_3$-labeled proteins, present considerable challenges for the design of Carr−Purcell−Meiboom−Gill (CPMG) relaxation dispersion NMR experiments to characterize chemical exchange on the micro-to-millisecond time-scale. Several approaches have been previously proposed for the elimination of deleterious artifacts observed in methyl ^{1}H CPMG relaxation dispersion profiles obtained for $(^{13}C)^{1}H_3$ groups. We describe an alternative, experimentally simple solution and design a "steady-state" methyl ^{1}H CPMG scheme, where 90° or acute-angle (<90°) ^{1}H radiofrequency pulses are applied after each CPMG echo in-phase with methyl ^{1}H magnetization, resulting in the establishment of a "steady-state" for effective rates of magnetization decay. A simple computational procedure for quantitative analysis of the "steady-state" CPMG relaxation dispersion profiles is developed. The "steady-state" CPMG methodology is applied to two protein systems where exchange between major and minor species occurs in different regimes on the chemical shift time-scale.

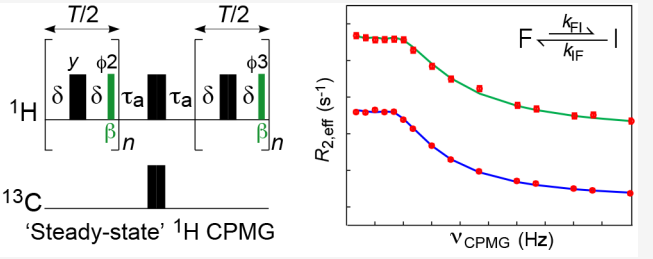

Downloaded via Gideon Clore on November 30, 2022 at 17:42:10 (UTC).
See https://pubs.acs.org/sharingguidelines for options on how to legitimately share published articles.

NMR spectroscopy is a powerful tool for studying chemical exchange processes in proteins.[1−4] For exchange processes occurring on the micro-to-millisecond time-scale, Carr−Purcell−Meiboom−Gill (CPMG) schemes[5,6] that modulate the effects of chemical exchange by application of a variable number of refocusing (180°) radiofrequency (RF) pulses during a constant time period are usually the method of choice.[4,7−9] Analysis of exchange-induced changes in nuclear relaxation rates as a function of the frequency of application of refocusing pulses (relaxation dispersion profiles) allows the kinetics of exchange to be quantified. Methyl-bearing side-chains in the hydrophobic cores of protein structures play a special role in these studies.[10] Considerable efforts have been devoted in the last two decades to developing CPMG NMR experiments that use selectively ^{13}C-labeled methyl groups as probes of exchange processes on the microsecond−millisecond time-scale.[11,12] One subclass of these experiments targets the three magnetically equivalent ^{1}H spins (A_3 spin-systems) in selectively $^{13}CH_3$-labeled proteins on a highly deuterated background.[13−15] Methyl ^{1}H chemical shifts may be more sensitive to environment than those of other nuclei/sites, making them particularly attractive probes of microsecond−millisecond dynamics.

The H_3 spin-system of a methyl group, however, presents considerable challenges for the design of CPMG experiments, as the completely degenerate ^{1}H transitions of such spin-systems have vastly different relaxation rates in the macromolecular limit. Accumulation of even minor imperfections of the refocusing ^{1}H RF pulses during the CPMG pulse-train can intermix the slow- and fast-relaxing components of methyl ^{1}H magnetization, leading to artifactual relaxation dispersion profiles even in the absence of exchange.[13,14,16] Several solutions to this problem have been previously suggested, in addition to recording ^{1}H relaxation dispersions on $^{13}CHD_2$ methyl isotopomers.[17] One solution involves isolation of ^{1}H transitions belonging to the $I = 1/2$ manifold of the $^{13}CH_3$ spin-system, which behaves as a ^{13}C−^{1}H moiety.[13,15] This approach, however, is associated with large sensitivity losses. Alternatively, methyl multiple-quantum (^{13}C−^{1}H) and single-quantum ^{13}C relaxation dispersion profiles may be analyzed simultaneously for extraction of changes in methyl ^{1}H chemical shifts.[16] This approach may be not as robust as direct recording of methyl ^{1}H CPMG data. Another ingenious solution was recently suggested by Kay and co-workers and

Received: September 25, 2022
Accepted: November 21, 2022

ACS Publications
Not subject to U.S. Copyright. Published XXXX by American Chemical Society

amounts to the application of a constant number of compensatory pulses during the CPMG relaxation delays that effectively "average out" the nonidealities of the refocusing pulses making them independent of CPMG frequency.[14] This CPMG scheme (dubbed "compensated CPMG" in the current paper) is methyl-TROSY[18] based and geared primarily toward very high molecular weight proteins.[14] Here, we describe another technically simple, alternative approach involving the design of a methyl ^{1}H CPMG scheme, where 90° or acute (<90°) ^{1}H RF pulses are applied after each CPMG echo in-phase with methyl ^{1}H magnetization, and develop a procedure for quantitative analysis of the resulting relaxation dispersion profiles.

Figure 1 shows the energy level diagram of a spin system consisting of three magnetically equivalent nuclei in a methyl group (H_3). Although $^{13}CH_3$ methyl groups are used in practice, ^{13}C transitions are omitted from the diagram for simplicity. The energy level diagram contains one manifold with spin $I = 3/2$ and two with $I = 1/2$. All five ^{1}H transitions in Figure 1 are completely degenerate and give rise to a single peak in the NMR spectrum. In the macromolecular limit, transverse spin relaxation of the inner ^{1}H transitions of both manifolds occurs with slower rates ($R_S^{3/2}$ for the $I = 3/2$ and $R_S^{1/2}$ for the $I = 1/2$ manifold, shown with red and green arrows in Figure 1, respectively), while the outer ^{1}H transitions of the $I = 3/2$ manifold (R_F, blue arrows) have much faster rates of decay.[18] Triple-quantum (TQ) ^{1}H transitions between the states $|1\rangle$ and $|4\rangle$ relax with a distinct rate, R_{TQ} (black arrows).

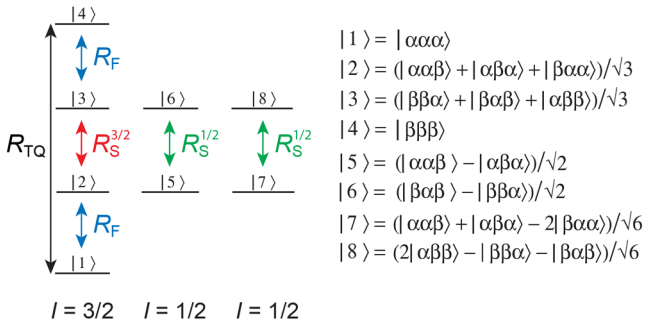

Figure 1. Energy level diagram of the X_3 spin-system of a methyl group. Slow-relaxing single-quantum ^{1}H transitions belonging to the $I = 3/2$ and $I = 1/2$ manifolds are shown by the red and green vertical arrows, respectively. Fast-relaxing (R_F) and triple-quantum (TQ) transitions are shown with blue and black arrows, respectively. The spin quantum numbers, I, of the three manifolds are specified below the diagram. The eight ^{1}H eigenstates described by linear combinations of $|i, j, k\rangle$ ($i, j, k \in \{\alpha, \beta\}$) are shown on the right.

The "steady-state" pulse scheme for recording methyl ^{1}H CPMG relaxation dispersion in $^{13}CH_3$ methyl groups is shown in Figure 2A. The experiment employs a heteronuclear multiple quantum coherence (HMQC) "read-out" scheme[19,20] with active selection of the slow-relaxing, inner methyl ^{1}H transitions (shown by the red and green vertical arrows in Figure 1) by the element of duration $2\tau_b$.[21] The constant-time CPMG period of total duration T is subdivided into two parts to "equalize" the relaxation rates of methyl ^{1}H magnetization in-phase and anti-phase with respect to methyl ^{13}C spins. Each CPMG echo (the period enclosed in square brackets in Figure 2A) is followed by an ^{1}H RF pulse applied with a variable flip-angle β with the phase collinear to that of the ^{1}H magnetization and cycled ±180° with retention of the receiver phase (shown in green in Figure 2A and referred to as the "β pulse" in the following).

It is instructive to consider first the effects of application of only a few β pulses on the relaxation of the signal (S) detected at the end of the experiment. Analytical expressions for methyl signal intensity I, obtained after application of n = 1, 2, and 3 β pulses during the relaxation delay T for β = 90° and 54.7° ("magic" angle) are shown in Figure 2B. The coefficients before each exponential term in Figure 2B for β = 54.7° are shown in italics (colored in magenta) and enclosed in curly brackets. While relaxation during the period T is biexponential after the application of a single β pulse, it becomes multiexponential and more complex as the number of pulses (n) grows (Figure 2B). It can be shown that the total number of exponential terms grows as $(n + 1)$ if the terms including R_{TQ} (O^n_{TQ}) are excluded, and as $(1/2)(n^2 + 3n)$ for all terms. As a result, the rates of decay of methyl magnetization may only be classified as "apparent" effective rates, $R^{app}_{2,eff} = -(1/T)\ln(I/I_0)$, where I_0 is initial signal intensity (at $T = 0$). It is also clear from the comparison of pre-exponential factors before the fast-(R_F) and slow-(R_S)-relaxing terms for β = 90° and 54.7° in Figure 2B, that for small n, the relative weights of the slow-relaxing terms increase for smaller (<90°) angles β (e.g., the ratio of the slow-to-fast weights is 1 and 2 for β = 90° and 54.7°, respectively, for n = 1; and 3/2 and 9/4 for β = 90° and 54.7°, respectively, for n = 2). For larger n, the intensities of the detected signal and, as a consequence, the rates $R^{app}_{2,eff}$, will converge to some limiting, "steady-state" values, with the rate of this convergence dictated by the choice of angle β (see below and the Supporting Information). In the following, we drop, for simplicity, the superscript "app" from the notation for effective R_2 rates.

We first ascertained that flat relaxation dispersion profiles are obtained in the experiment of Figure 2A in the absence of exchange. The profiles, simulated on-resonance and in the absence of exchange using the full density matrix representation in the basis of Figure 1 as a function of the number of β pulses n, are shown in Figure 3A. As expected, when the β pulses are omitted, the imperfections of the ^{1}H 180° pulses accumulate with the number of CPMG echoes leading to growing dispersion profiles even in the absence of exchange (cf. solid green curve and dashed green line in Figure 3A). This behavior of methyl ^{1}H CPMG profiles has been documented in the literature.[13,14,16] Inclusion of the β pulses largely "flattens" the profiles in the absence of exchange, with small residual oscillations of $R_{2,eff}$ observed at the beginning of the profiles before the "steady-state" is achieved (black, blue, and red curves). Importantly, these profiles are completely insensitive to imperfections of refocusing (180°) pulses in the CPMG pulse-train and are indistinguishable from each other irrespective of the value by which the refocusing pulses are mis-set. Note that in practice, the first CPMG frequency, ν_{CPMG}, sampled in the experiment of Figure 2A corresponds to 4 β pulses (n = 4 and nc = 2 in Figure 2A; marked by the vertical dashed line in Figure 3A). It is also noteworthy that lower values of the angle β change the convergence properties of the profiles somewhat (Figure 3A) by increasing the relative contribution of the slow-relaxing coherences to the detected signal (Figure 2B). Figure 3B shows typical experimental relaxation dispersion profiles obtained for ILV methyls of ubiquitin (5 °C; rotational correlation time τ_C in $D_2O \approx 11$ ns) and Ileδ1 methyls of Malate Synthase G (MSG, 37 °C; $\tau_C \approx 45$ ns), where no detectable exchange occurs. The lower

https://doi.org/10.1021/acs.jpclett.2c02937
J. Phys. Chem. Lett. 2022, 13, 11271−11279

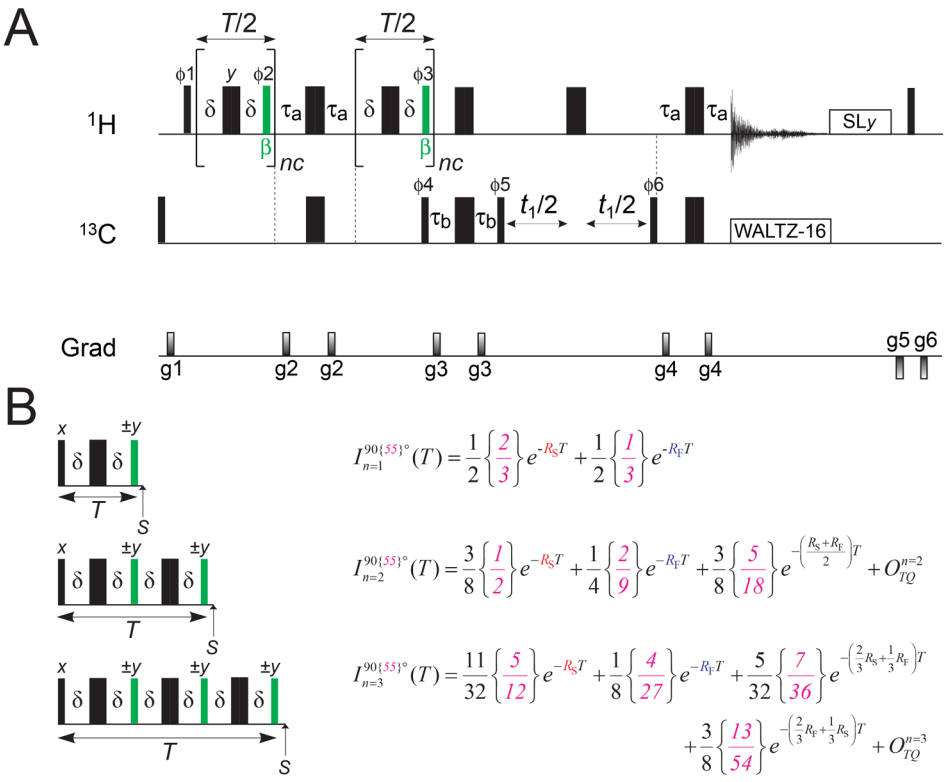

$$I_{n=1}^{90\{55\}^\circ}(T) = \frac{1}{2}\left\{\frac{2}{3}\right\}e^{-R_S T} + \frac{1}{2}\left\{\frac{1}{3}\right\}e^{-R_F T}$$

$$I_{n=2}^{90\{55\}^\circ}(T) = \frac{3}{8}\left\{\frac{1}{2}\right\}e^{-R_S T} + \frac{1}{4}\left\{\frac{2}{9}\right\}e^{-R_F T} + \frac{3}{8}\left\{\frac{5}{18}\right\}e^{-\left(\frac{R_S+R_F}{2}\right)T} + O_{TQ}^{n=2}$$

$$I_{n=3}^{90\{55\}^\circ}(T) = \frac{11}{32}\left\{\frac{5}{12}\right\}e^{-R_S T} + \frac{1}{8}\left\{\frac{4}{27}\right\}e^{-R_F T} + \frac{5}{32}\left\{\frac{7}{36}\right\}e^{-\left(\frac{2}{3}R_S+\frac{1}{3}R_F\right)T} + \frac{3}{8}\left\{\frac{13}{54}\right\}e^{-\left(\frac{2}{3}R_F+\frac{1}{3}R_S\right)T} + O_{TQ}^{n=3}$$

Figure 2. ^{1}H CPMG relaxation dispersion in $^{13}CH_3$ methyl groups. (A) Pulse scheme for recording ^{1}H CPMG relaxation dispersion in $^{13}CH_3$ methyl groups. All narrow and wide rectangular pulses are applied with flip-angles of 90° and 180°, respectively, along the *x*-axis unless indicated otherwise. The ^{1}H carrier is positioned in the center of the Ile$^{\delta1}$-Leu-Val (ILV) methyl region (0.4−0.5 ppm), while the ^{13}C carrier is positioned at 20 ppm for ILV-labeled samples. All ^{1}H and ^{13}C pulses are applied with the highest possible power, with WALTZ-16 ^{13}C decoupling[22] achieved using a 2.5 kHz RF field. The pulses shown in green are applied after each CPMG echo with a variable flip-angle β (see text). A ^{1}H spin-lock field (10 kHz, *y*-axis) is applied for 40 ms after acquisition ("SL$_y$"). This spin-lock and the subsequent ^{1}H purge pulse eliminate all transverse components of magnetization before the start of the experiment. Delays are as follows: $\tau_a = 1/(4^1J_{CH}) = 2.0$ ms; $\tau_b = 1/(8^1J_{CH}) = 1$ ms; and T is a constant time relaxation delay. An even number of CPMG cycles (nc) is employed. Phase cycling is as follows: $\phi1 = x, -x$; $\phi2 = 4(y), 4(-)$; $\phi3 = 4(x), 4(-x)$; $\phi4 = 2(x), 2(-x)$; $\phi5 = 2(y), 2(-y)$; $\phi6 = x$; receiver = $x, -x, -x, x$. The durations and strengths of pulsed-field *z*-gradients in units of (ms; G/cm) are g1 = (1; 40), g2 = (0.5; 20), g3 = (0.4; 30), g4 = (0.5; 25), g5 = (1.2; −25), g6 = (0.6; −25). Quadrature detection in F_1 is achieved by States-TPPI incrementation[23] of phase $\phi6$. Details of experimental parameters are provided in the Supporting Information. (B) Analytical expressions for the methyl signal intensity I obtained after application of 1, 2, and 3 variable angle β pulses (shown in green; phase-cycled $\pm y$) during the relaxation delay T. The signal detected at the end of each experiment (shown with vertical arrows and labeled "S") is assumed to consist of the central, slow-relaxing transitions only (red and green arrows in Figure 1). Relaxation of all methyl ^{1}H transitions is assumed to be single-exponential. The coefficients listed in the expressions on the right are for $\beta = 90°$, while those calculated for $\beta = 54.7°$ ("magic angle"; ∼55°) are shown in curly brackets, in italics, and colored in magenta. Relaxation rates of the slow-relaxing transitions of the $I = 3/2$ and $I = 1/2$ manifolds are assumed to be the same, $R_S^{3/2} = R_S^{1/2} = R_S$, for simplicity. The terms "O_{TQ}" include the relaxation rates R_{TQ}.

profiles for each methyl site in both proteins in Figure 3B are obtained with the scheme in Figure 2A with β pulses omitted. Application of β pulses, with β set to 90°, provides largely flat profiles, with only minor (<1 s^{-1}) oscillations at low CPMG frequencies. Very similar data were obtained for β set to 55° and 60° for ubiquitin and MSG methyls, respectively. In a sense, the convergence to the limiting value of $R_{2,\mathrm{eff}}$ is achieved in the absence of β pulses too (lower profiles in Figure 3B). The application of β pulses effectively accelerates this process at the expense of somewhat higher limiting ("steady-state") values of $R_{2,\mathrm{eff}}$. Below, we briefly summarize how these "steady-state" rates can be calculated in the absence of exchange.

The transformation corresponding to the application of a ^{1}H RF pulse with flip-angle β, $\tilde{P}_\beta$, applied with a phase collinear to that of methyl ^{1}H magnetization and phase-cycled as in Figure 2A, can be represented by the matrix operating on the column vector of magnetizations, $\vec{M}$

$$\tilde{P}_\beta\vec{M} = \frac{1}{4}\begin{bmatrix} (3+\cos 2\beta) & (1-\cos 2\beta) & (\cos 2\beta - 1) & 0 \\ (3/2)(1-\cos 2\beta) & (1/2)(5+3\cos 2\beta) & (3/2)(1-\cos 2\beta) & 0 \\ (3/2)(\cos 2\beta - 1) & (3/2)(1-\cos 2\beta) & (1/2)(5+3\cos 2\beta) & 0 \\ 0 & 0 & 0 & 4 \end{bmatrix}\vec{M};\ \vec{M} = \begin{bmatrix} F \\ S^{3/2} \\ TQ \\ S^{1/2} \end{bmatrix} \quad (1)$$

https://doi.org/10.1021/acs.jpclett.2c02937
J. Phys. Chem. Lett. 2022, 13, 11271−11279

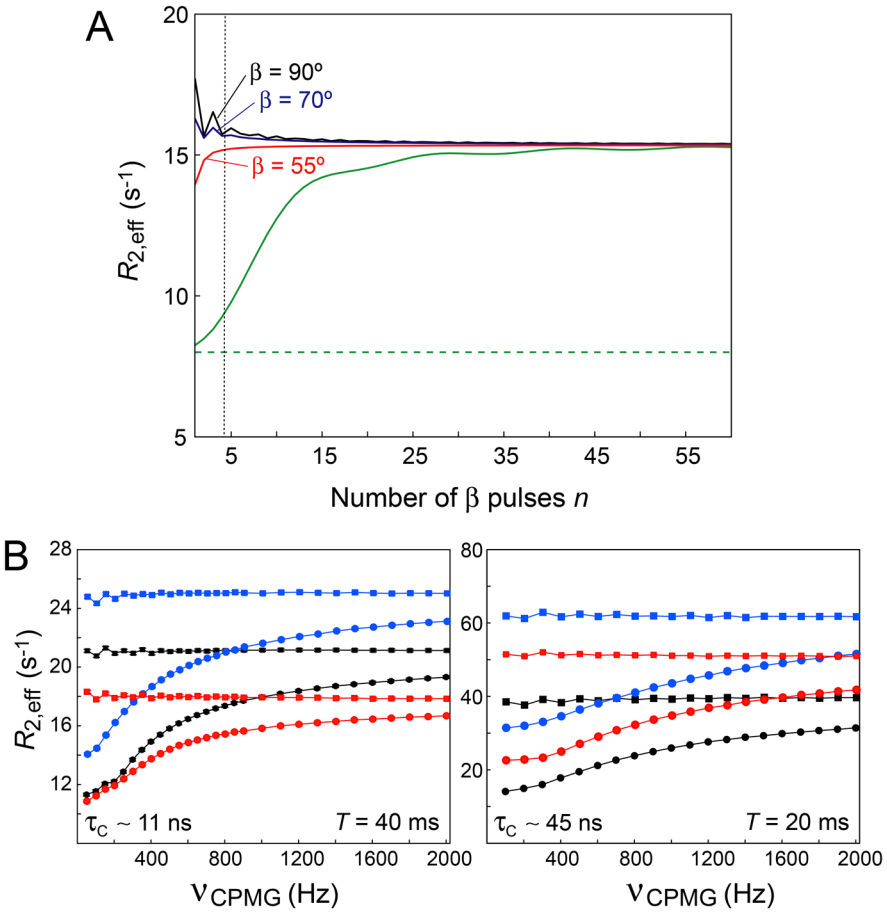

Figure 3. Effect of β pulses on methyl ^{1}H CPMG relaxation dispersion profiles in the absence of exchange. (A) Relaxation dispersion profiles simulated using the full density matrix representation in the basis of Figure 1 as a function of the number of β pulses n, in the absence of exchange and on-resonance. The dashed green line corresponds to the profile obtained for ideal 180° pulses during the CPMG period and β pulses omitted; the solid green curve was generated for 180° pulses during the CPMG period mis-set by 12° and β pulses omitted; the profiles shown in black, blue, and red were generated with β pulses included and phase-cycled as in Figure 2A, with β set to 90°, 70°, and 54.7°, respectively. The vertical dashed line is drawn at $n = 4$ (see text). The following parameters were used in the simulations: $R_F = 45$ s^{-1}; $R_S^{3/2} = R_S^{1/2} = R_S = 8$ s^{-1}; $R_{TQ} = 35$ s^{-1}; $T = 60$ ms. (B) Representative experimental dispersion profiles obtained in the absence of exchange for ILV methyls of ubiquitin (left panel, 5 °C; 8.5 kDa, $\tau_C \approx 11$ ns; $T = 40$ ms; 600 MHz) and Ileδ1 methyls of Malate Synthase G (right panel, 37 °C; 82 kDa, $\tau_C \approx 45$ ns; $T = 20$ ms; 600 MHz). $\nu_{CPMG} = nc/T$ (Figure 2A). The profiles for each methyl site are color coded with the same colors (black, red, or blue). Lower profiles (filled-in circles) in each case were obtained with the scheme in Figure 2A with β pulses omitted, while the upper ones (filled-in squares) were obtained with β pulses ($\beta = 90°$) included.

where $F = (\sqrt{3}/2)(|1\rangle\langle 2| + |2\rangle\langle 1| + |3\rangle\langle 4| + |4\rangle\langle 3|)$; $S^{3/2} = |2\rangle\langle 3| + |3\rangle\langle 2|$; $TQ = |1\rangle\langle 4| + |4\rangle\langle 1|$; and $S^{1/2} = (1/2)(|5\rangle\langle 6| + |6\rangle\langle 5| + |7\rangle\langle 8| + |8\rangle\langle 7|)$ in the basis of Figure 1, with initial conditions applicable to the ^{1}H CPMG experiment in Figure 2A, namely, $\vec{M}(0) = [1, 1, 0, 1]^T$, where "T" denotes transposition. This "vectorization" of the density matrix is possible due to elimination of all other matrix elements (double-quantum ^{1}H coherences and populations) by the phase-cycling of β pulses (see the Supporting Information). In the Supporting Information, we show that for a large number of β pulses n, the value of $(\tilde{P}_\beta)^n$ reaches a "steady-state" described by the matrix $\tilde{P}_{ID}$, which is idempotent (i.e., $(\tilde{P}_\beta)^n = \tilde{P}_\beta$ for any positive integer n). In the framework of eq 1, for the initial conditions stated above and *any* flip-angle β, the limit of convergence, $\vec{M}_L$, for all components of the magnetization in $\vec{M}$ (and hence for the "apparent", effective rates $R_{2,eff}$) can be described by a simple transformation

$$\vec{M}_L = e^{-\tilde{P}_{ID}\tilde{R}_r T}\vec{M}(0) = e^{-\tilde{P}_{45°}\tilde{R}_r T}\vec{M}(0) \quad (2)$$

where the idempotent matrix $\tilde{P}_{ID}$ is equivalent to the matrix for $\beta = 45°$, $\tilde{P}_{45°}$; and $\tilde{R}_r$ is the relaxation matrix for the vector of magnetizations $\vec{M}$, which in its simplest form (if cross-relaxation between the fast- and slow-relaxing transitions is neglected) is diagonal, $diag([R_F, R_S^{3/2}, R_{TQ}, R_S^{1/2}])$; see the Supporting Information for a more general expression for $\tilde{R}_r$ in the macromolecular limit. The effective rates $R_{2,eff}$ of the magnetization detected at the end of the experiment in Figure 2A in the absence of exchange can then be estimated from the limit in eq 2 as $R_{2,eff} = -(1/T)\ln(I/I_0)$, where $I = 2\vec{M}_L[2] + \vec{M}_L[4]$, and I_0 is initial signal intensity (at $T = 0$), $I_0 = 2\vec{M}[2](0) + \vec{M}[4](0)$. Of note, such "steady-state" rates are predicted to be weakly, inversely dependent on the choice of T, with *shorter* delays T leading to very minor *increases* in $R_{2,eff}$ (Figure S1). Figure S2 shows how the "steady-state" dispersion profiles simulated in the absence of exchange are modulated at low CPMG frequencies by the angle β.

Even in the reduced, "vectorized" framework of eq 1, the evolution of methyl ^{1}H magnetization during the time period T of the scheme in Figure 2A involves too many relaxation rates

https://doi.org/10.1021/acs.jpclett.2c02937
J. Phys. Chem. Lett. 2022, 13, 11271−11279

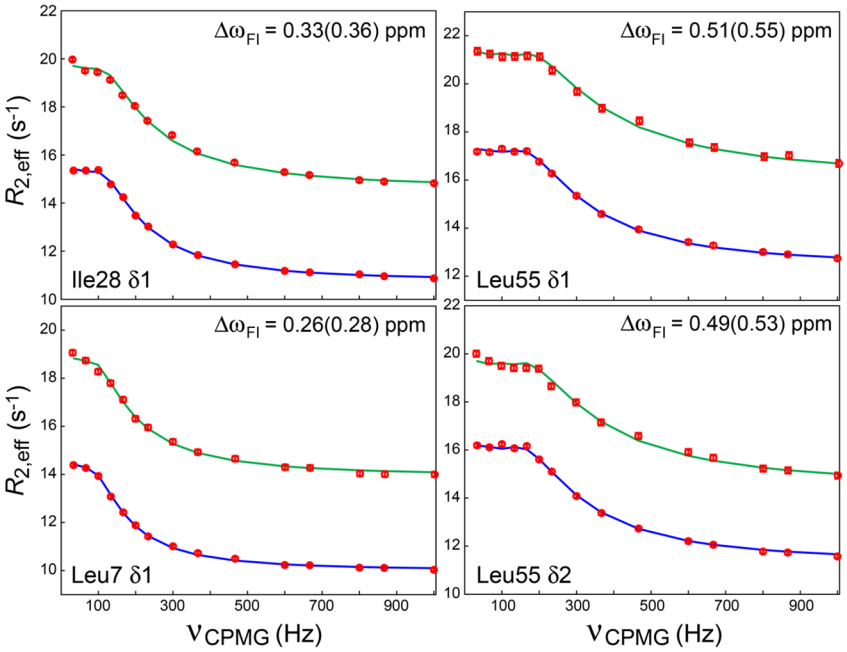

Figure 4. Selected ^{1}H CPMG relaxation dispersion profiles obtained for methyl sites of {U-[^{2}H]; Ileδ1-[$^{13}CH_3$]; Leu,Val-[$^{13}CH_3$,$^{12}CD_3$]}-labeled Fyn SH3^{VPL} (600 MHz; 10 °C). All experimental points are shown with red circles. Lower profiles in each panel (fitted with blue curves) were obtained with the compensated methyl TROSY-based ^{1}H CPMG scheme of Yuwen et al.[14] Upper profiles (fitted with green curves) were obtained with the "steady-state" ^{1}H CPMG experiment in Figure 2A with the β angle set to 55°. The fitted values of $|\Delta\omega_{FI}|$ for each methyl site are shown in the right top corner of each panel, with the values obtained in the "steady-state" experiment indicated in parentheses. See the Supporting Information for experimental details and sample conditions.

that cannot be obtained with confidence from analysis of relaxation dispersion profiles. A simplified "model" of relaxation is therefore in order for robust characterization of exchange processes. In the following, we describe how such a "model" can be constructed for analysis of "steady-state" ^{1}H relaxation dispersions. Under the assumptions that (1) no cross-relaxation occurs between the fast- and slow-relaxing components of $\vec{M}$; (2) $R_{TQ} = R_F$; and (3) $R_S^{3/2} = R_S^{1/2} = R_S$, the relaxation matrix $\tilde{R}_r$ simplifies to, $\tilde{R}_r^s = diag([R_F, R_S, R_F, R_S])$. Applying the transformation in eq 2 to the vector of initial conditions $\vec{M}(0) = [1, 1, 0, 1]^T$ and retaining only the part of magnetization that contributes to the signal detected at the end of the experiment in Figure 2A, $(2\vec{M}[2] + \vec{M}[4])$, yields the "steady-state" rate

$$R_{2,\mathrm{eff}}^{ss} = -\frac{1}{T}\ln\left\{\frac{2}{3}e^{-\left[\frac{5}{8}R_S+\frac{3}{8}R_F\right]T} + \frac{1}{3}e^{-R_S T}\right\} \quad (3)$$

where the superscript "ss" is introduced to distinguish the rate estimated with eq 3 from that calculated using the full relaxation matrix. As described in the Supporting Information, these estimated "steady-state" rates are reasonably good approximations to the rates obtained with the full matrix $\tilde{R}_r$. For further reduction in the number of variable parameters in analysis of "steady-state" dispersion profiles, we express both R_S and R_F as multiples of $R_{2,\mathrm{eff}}^{ss}$, $R_S = f_S R_{2,\mathrm{eff}}^{ss}$ and $R_F = f_F R_{2,\mathrm{eff}}^{ss}$, where $\sim 0.25 < f_S < 1$, and $f_F > 1$. It is advantageous to fix the coefficient f_F to a predetermined value (see the Supporting Information for the procedure we used to find an estimate of f_F and pertinent details), and find the corresponding value for f_S by searching for the zero of the function F

$$F = \frac{2}{3}e^{-\left[\frac{3}{8}f_F+\frac{5}{8}f_S-1\right]R_{2,\mathrm{eff}}^{ss}T} + \frac{1}{3}e^{(1-f_S)R_{2,\mathrm{eff}}^{ss}T} - 1 \quad (4)$$

Figure S3 shows the plot of f_S versus f_F for methyl groups of proteins of different sizes obtained by a numerical search for zero in F. The ratio, $f_F/f_S = R_F/R_S$, serves as a measure of separation between the fast and slow rates of decay in the $(^{13}C)H_3$ spin-system.

The performance of the experiment in Figure 2A in the presence of exchange was tested on a triple A39V/N53P/V55L (VPL) mutant of the Fyn SH3 domain. This system was characterized previously by a variety of exchange NMR techniques and shown to spontaneously unfold through a well-defined intermediate state in a temperature-dependent manner.[24,25] At 10 °C, the population of the unfolded state is too low to be detected, and exchange at this temperature can be adequately described by a 2-site equilibrium between the folded (F) and intermediate (I) states, $F \underset{k_{IF}}{\overset{k_{FI}}{\rightleftharpoons}} I$.[24,26] The values of $k_{FI} = 7.1 \pm 0.1$ s^{-1} and $k_{IF} = 258 \pm 11$ s^{-1} reported previously for a ^{15}N-labeled/protonated sample of Fyn SH3^{VPL} from ^{15}N relaxation dispersion experiments translate to a fractional population (p_I) of 2.7 ± 0.14% for the folding intermediate with an overall exchange rate of $k_{ex} = k_{FI} + k_{IF} = 265 \pm 12$ s^{-1}.[24]

For the two-state exchange in Fyn SH3^{VPL}, the time evolution of the magnetization vector $\vec{M}^{2\text{-site}} = \hat{I}_2 \otimes \vec{M}$, where $\hat{I}_2$ is a 2 × 2 unity matrix and "⊗" denotes the Kronecker product, during the CPMG time period T in the experiment of Figure 2A, is calculated as

$$\vec{M}^{2\text{-site}}(T) = (\tilde{P}_\beta^{2\text{-site}}\tilde{A}\tilde{A}^*\tilde{P}_\beta^{2\text{-site}}\tilde{A}^*\tilde{A})^{nc}\vec{M}^{2\text{-site}}(0) \quad (5)$$

where $\tilde{A} = \exp(-\tilde{R}^{2\text{-site}}\delta)$; $\tilde{A}^*$ is the complex conjugate of $\tilde{A}$; nc is the number of CPMG cycles employed ($nc = n/2$, where n is the number of β pulses); δ is one-half of the time-period

https://doi.org/10.1021/acs.jpclett.2c02937
J. Phys. Chem. Lett. 2022, 13, 11271−11279

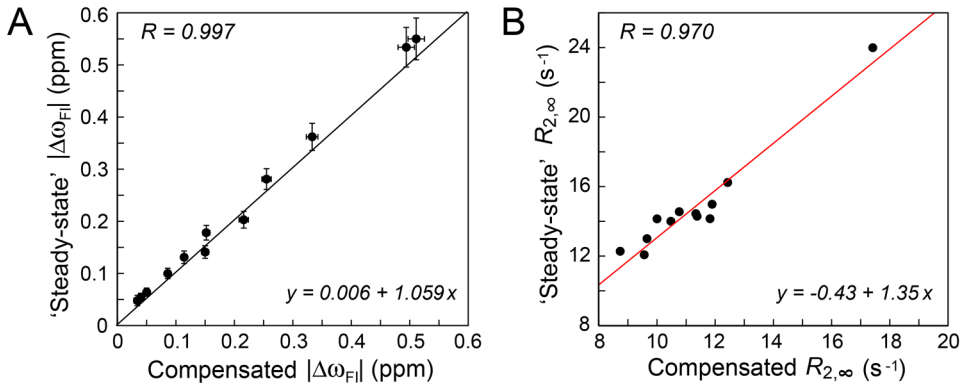

Figure 5. Correlation plots comparing (A) the absolute differences in methyl ^{1}H chemical shifts between the folded (F) and intermediate (I) states, $|\Delta\omega_{FI}| = |\omega_I - \omega_F|$ (ppm), and (B) the fitted R_2 rates in the limit $\nu_{CPMG} \rightarrow \infty$, $R_{2,\infty}$ (s^{-1}), obtained for 12 methyl groups of {U-[^{2}H]; Ileδ1-[$^{13}CH_3$]; Leu,Val-[$^{13}CH_3$,$^{12}CD_3$]}-labeled Fyn SH3^{VPL}, with the compensated CPMG scheme (x-axes) and the "steady-state" CPMG experiment in Figure 2A (y-axes). The parameters of linear regression are indicated in the plots. The black line in panel A corresponds to $y = x$, while the red line in panel B is drawn using the parameters of linear regression indicated at the bottom of the panel.

between two consecutive 180° pulses (Figure 2A); $\tilde{P}_\beta^{2\text{-site}} = \hat{I}_2 \otimes \tilde{P}_\beta$; and $\vec{M}^{2\text{-site}}(0) = [p_F, p_I]^T \otimes \vec{M}(0)$. The Liouvillian propagated in the calculations of methyl ^{1}H relaxation dispersion profiles is composed of 3 matrices: $\tilde{R}^{2\text{-site}} = \tilde{R}_r^{2\text{-site}} + \tilde{R}_{cs}^{2\text{-site}} + \tilde{R}_{ex}^{2\text{-site}}$, where $\tilde{R}_r^{2\text{-site}} = \hat{I}_2 \otimes \tilde{R}_r^s$; $\tilde{R}_{cs}^{2\text{-site}}$ is the diagonal matrix of the changes in chemical shifts between the states I and F ($\Delta\omega_{FI} = \omega_I - \omega_F$), $\tilde{R}_{cs}^{2\text{-site}} = diag(-i[0\ 0\ 0\ 0\ \Delta\omega_{FI}\ \Delta\omega_{FI}\ 3\Delta\omega_{FI}\ \Delta\omega_{FI}])$, and $\tilde{R}_{ex}^{2\text{-site}}$ is the exchange matrix

$$\tilde{R}_{ex}^{2\text{-site}} = -\begin{bmatrix} k_{FI} & -k_{IF} \\ -k_{FI} & k_{IF} \end{bmatrix} \otimes \hat{I}_4 \qquad (6)$$

where $\hat{I}_4$ is a 4×4 unity matrix. The rates R_F and R_S that enter into the simplified relaxation matrix $\tilde{R}_r^s$, are expressed as multiples of the steady-state rate $R_{2,eff}^{ss}$ that serves as a variable parameter in the fit (see above). The factor f_F is estimated from the ratio $\langle R_F\rangle/\langle R_{2,eff}^{ss}\rangle$ (where the average rate R_F for all methyl sites included in analysis, $\langle R_F\rangle$, is measured separately and corrected for R_{ex} as described in the Supporting Information), while the value of f_S can be found from the zero of the function F in eq 4.

We recorded several ^{1}H CPMG relaxation dispersion profiles for ILV methyl sites of {U-[^{2}H]; ILV-[$^{13}CH_3$]}-labeled Fyn SH3^{VPL} dissolved in D_2O (10 °C) using the scheme in Figure 2A with the flip-angles of the β pulses adjusted to 90°, 70°, 60°, and 55° ("magic" angle value of 54.7° rounded to the next integer). Although the differences between these data sets are quite small, the data obtained with $\beta = 55°$ proved the best in terms of the quality of dispersion profiles and agreement with the compensated ^{1}H CPMG scheme. Selected relaxation dispersion profiles obtained with the "steady-state" CPMG experiment ($\beta = 55°$) are compared in Figure 4 with those obtained under identical experimental conditions with the compensated CPMG scheme. Additional profiles for methyl sites with $R_{ex} > \sim 2\ s^{-1}$ are provided in Figure S4. The "steady-state" data were analyzed as described above using a uniform value of f_F set to 1.9 (no improvements in the fit were observed with residue-specific values of f_F) and the angle β set to 55° in eq 5. Notably, the shapes of the profiles for the two experiments are very similar, with the "steady-state" experiment (upper curves in Figure 4) providing $R_{2,eff}$ rates offset upward approximately by the same value for all ν_{CPMG} frequencies, and hence yielding the same R_{ex} as well as information content. A global fit to CPMG relaxation dispersion profiles for 12 methyl groups with $R_{ex} > 1\ s^{-1}$ provided very similar values for the two experiments: $k_{FI} = 5.1 \pm 0.1$ and $5.2 \pm 0.2\ s^{-1}$ and $k_{IF} = 288 \pm 20$ and $246 \pm 30\ s^{-1}$ for the compensated and "steady-state" experiments, respectively, translating to $p_I = 1.7 \pm 0.13\%$ and $2.1 \pm 0.3\%$, respectively, and $k_{ex} = 293 \pm 21$ and $251 \pm 32\ s^{-1}$, respectively, for the two experiments. We note that relatively high uncertainties obtained for k_{IF} (and p_I) are a hallmark of exchange that occurs slowly on the chemical shift time-scale for the majority of methyl sites ($k_{ex} < |\Delta\omega_{FI}|$). This regime makes the characterization of exchange by the "steady-state" experiment particularly challenging, as it requires a good description of the initial portions of CPMG profiles (at low ν_{CPMG}) where the "steady-state" relaxation rates may not be yet completely attained. Generally, the "steady-state" CPMG experiment yields data of slightly inferior quality—especially for the first several points at the lowest ν_{CPMG}, where the "steady-state" condition is not completely satisfied, which is reflected in a slightly higher χ^2 of the fit for the "steady-state" scheme ($\chi^2 = 2.87$) compared to that for the compensated one ($\chi^2 = 2.49$).

Excellent correlations are obtained for the differences in methyl ^{1}H chemical shifts between the states F and I, $|\Delta\omega_{FI}|$, for the two experiments (Figure 5A), with the "steady-state" experiment overestimating $\Delta\omega$ only very slightly (~6%). The fitted R_2 rates in the limit, $\nu_{CPMG} \rightarrow \infty$, $R_{2,\infty}$, in the two experiments are also highly linearly correlated, with the "steady-state" $R_{2,\infty}$ rates higher than those from the compensated experiment by ~35% (Figure 5B). Such an increase in the $R_{2,\infty}$ rate is not expected to be prohibitive for small-to-intermediate sized proteins. For higher molecular weight systems, however, these "steady-state" rates will grow proportionately. For example, for proteins the size of malate synthase G ($\tau_C \approx 45$ ns; see examples in Figure 3B, right panel) the average $R_{2,\infty}$ over all Ileδ1 methyl sites, $\langle R_{2,\infty}\rangle$, is ~2.5-fold higher than the relaxation rates of the slow-(R_S)-relaxing ^{1}H transitions that would be observed at the end of NMR experiments. This constitutes the principal limitation of the "steady-state" CPMG experiment, as higher $R_{2,\infty}$ rates would restrict the length of relaxation delays T to prohibitively short values.

It is of interest to compare the sensitivities of the "steady-state" and compensated CPMG schemes. We note that at least

https://doi.org/10.1021/acs.jpclett.2c02937
J. Phys. Chem. Lett. 2022, 13, 11271−11279

in the absence of differential relaxation in the H_3 spin-system, the β pulses do not have any adverse effects on the sensitivity of the experiment in Figure 2A,[27] irrespective of the angle β used (in practice, β cannot be much smaller than ∼50°, see the Supporting Information). In practice, we found that the sensitivity of the "steady-state" experiment is ∼3/4 of that for the compensated scheme for Fyn SH3^{VPL} (10 °C), primarily because both fast- and slow-relaxing ^{1}H coherences are detected in the latter, whereas in the former, the fast-relaxing components of ^{1}H magnetization are "filtered out" prior to signal acquisition. Although slightly inferior in sensitivity and quality of relaxation dispersion profiles to the compensated CPMG experiment, the "steady-state" scheme is simpler in technical implementation; does not involve composite ^{1}H 180° pulses with extensive, complicated phase-cycling during the CPMG periods (see discussion in the Supporting Information); and considerably reduces the duty cycle on the ^{1}H channel of the NMR spectrometer. Importantly, numerical simulations predict that the "steady-state" experiment would preserve the values of R_{ex} (and therefore the information content of CPMG relaxation dispersion profiles) for any regime of exchange, whereas a slight decrease in R_{ex} is expected for the compensated scheme when exchange approaches the fast limit on the chemical shift time-scale.[14] It is worth noting that very similar parameters of exchange are extracted from relaxation dispersions obtained for Fyn SH3^{VPL} with the experiment that selects for ^{1}H transitions of the $I = 1/2$ manifold,[15] albeit with almost a 3-fold loss in sensitivity.

While the transformation in eq 1 is useful for (a) analysis of the "steady-state" CPMG relaxation dispersion profiles and (b) the derivation of the limiting ("steady-state") value of the effective relaxation rates, $R_{2,eff}$, it is not applicable to analysis of off-resonance effects and mis-calibration of CPMG 180° pulses. We carried out estimates of the effects of mis-calibration of the "steady-state" CPMG pulses in the presence of off-resonance effects (methyl ^{1}H chemical shifts offset from the carrier position) and in the absence of exchange, using the full density matrix of the (^{13}C)H_3 spin-system in the basis of Figure 1. We note that, off-resonance, acute angle (<90°) ^{1}H β pulses consistently perform better than 90° pulses in ensuring the stability of the "steady-state" R_2 rates. For an offset of ±0.5 ppm (300 Hz at 600 MHz) from the ^{1}H carrier (note that there is only one methyl site in Fyn SH3^{VPL} that has a larger offset: Ile50δ1; Figure S4) and for magic-angle β pulses (55°), we calculate that mis-calibration of the CPMG 180° pulses up to ∼1.5% (∼2.5°) can be tolerated (i.e., the changes in the "steady-state" R_2 rates are likely to be within the uncertainties of the measurement). Although the "steady-state" experiment is predicted to be less "forgiving" with respect to pulse mis-calibration in the presence of off-resonance effects than its compensated counterpart,[14] and composite ^{1}H RF pulses cannot mitigate these effects (see the Supporting Information for discussion), we estimate that on state-of-the-art NMR spectrometers used for biological applications, ^{1}H pulses can be calibrated to an accuracy of ∼0.5% or better (∼0.2 μs or lower for a 360° pulse).

To test the performance of the "steady-state" scheme for a higher molecular weight protein involving a much faster regime of exchange on the chemical shift time-scale, we applied the experiment in Figure 2A to the 25-kDa chaperone construct ΔST-DNAJB6B.[28] At concentrations above ∼100 μM, ΔST-DNAJB6B undergoes spontaneous oligomerization and interconverts between the free monomeric state and high molecular weight oligomers comprising ∼35−40 monomeric units.[28] Our earlier methyl ^{13}C CPMG relaxation dispersion study on ΔST-DNAJB6B at 15 °C yielded an exchange rate k_{ex} of 1050 ± 60 s^{-1} and a fractional population p_B for the oligomeric species of 4.7 ± 0.4%.[29] Because of the small number of methyl probes that undergo exchange with sufficiently large changes in ^{1}H chemical shifts, we fixed k_{ex} to 1000 s^{-1} in global fits of methyl ^{1}H CPMG data to obtain p_B of 3.7 ± 0.5% and 3.8 ± 0.4% with the "steady-state" (β = 90°) and compensated CPMG schemes, respectively. The "steady-state" CPMG data were analyzed with f_F set to 1.6 reflecting a high degree of mobility of ΔST-DNAJB6B methyl sites participating in exchange[28] (see Figure S5 for relaxation dispersion profiles for two methyl sites of ΔST-DNAJB6B with the largest chemical shift differences between the free and oligomer-bound species ($\Delta\omega$); Table S1 comparing methyl ^{1}H $\Delta\omega$ values obtained from the compensated and "steady-state" experiments; and the Supporting Information "Materials and Methods" for sample conditions, acquisition parameters, and details of analysis used for ΔST-DNAJB6B).

In summary, we describe an experimentally simple "steady-state" methyl ^{1}H CPMG scheme for quantification of chemical exchange in selectively [$^{13}CH_3$]-labeled and otherwise deuterated proteins. The "steady-state" for effective rates of magnetization decay is achieved by application of a 90° or acute-angle (<90°) ^{1}H RF pulses after each CPMG echo, in-phase with methyl ^{1}H magnetization. Application of in-phase 90° ^{1}H RF pulses in CPMG echoes was described previously in chemical NMR applications for the purpose of eliminating the effects of scalar (J) couplings.[30−33] In the "steady-state" CPMG experiment, these ^{1}H pulses play a completely different role, effectively establishing a "steady-state" in the decay of methyl ^{1}H magnetization components relaxing with very different rates. A procedure developed for quantitative analysis of the "steady-state" CPMG relaxation dispersion profiles allowed us to characterize the exchange process between the folded state of Fyn SH3^{VPL} and a folding intermediate occurring in a regime that is slow exchange on the chemical shift time-scale and exchange between monomeric and oligomeric species of the chaperone ΔST-DNAJB6B on a much faster time-scale.

■ ASSOCIATED CONTENT

Data Availability Statement

The Matlab scripts, used in global fitting of "steady-state" CPMG relaxation dispersion data, have been deposited on figshare (Tugarinov, V. Analysis of 'Steady-state' Methyl ^{1}H CPMG Relaxation Dispersion Profiles. 10.6084/m9.figshare.21538452.v1, deposited November 10, 2022).

Supporting Information

The Supporting Information is available free of charge at https://pubs.acs.org/doi/10.1021/acs.jpclett.2c02937.

Derivation of eq 1 and derivation of the "steady-state" limits for the apparent $R_{2,eff}$ rates for any flip-angle β in eq 2; justification for the simplifying assumptions used in analysis of the "steady-state" relaxation dispersion profiles; discussion of some practical aspects of the "steady-state" CPMG experiment; Materials and Methods describing NMR sample conditions, NMR acquisition parameters, and details of data analysis (PDF)

https://doi.org/10.1021/acs.jpclett.2c02937
J. Phys. Chem. Lett. 2022, 13, 11271−11279

AUTHOR INFORMATION

Corresponding Authors

Vitali Tugarinov − *Laboratory of Chemical Physics, National Institute of Diabetes and Digestive and Kidney Diseases, National Institutes of Health, Bethesda, Maryland 20892-0520, United States*; Email: vitali.tugarinov@nih.gov

G. Marius Clore − *Laboratory of Chemical Physics, National Institute of Diabetes and Digestive and Kidney Diseases, National Institutes of Health, Bethesda, Maryland 20892-0520, United States*; orcid.org/0000-0003-3809-1027; Email: mariusc@mail.nih.gov

Authors

Yusuke Okuno − *Laboratory of Chemical Physics, National Institute of Diabetes and Digestive and Kidney Diseases, National Institutes of Health, Bethesda, Maryland 20892-0520, United States*

Francesco Torricella − *Laboratory of Chemical Physics, National Institute of Diabetes and Digestive and Kidney Diseases, National Institutes of Health, Bethesda, Maryland 20892-0520, United States*

Theodoros K. Karamanos − *The Astbury Center for Structural Molecular Biology, School of Molecular and Cellular Biology, University of Leeds, Leeds LS2 9JT, U.K.*; orcid.org/0000-0003-2297-540X

Complete contact information is available at: https://pubs.acs.org/10.1021/acs.jpclett.2c02937

Notes

The authors declare no competing financial interest.

ACKNOWLEDGMENTS

We thank Prof. Lewis Kay (University of Toronto, Canada) for useful discussions and suggestions. The authors thank Dr. Alberto Ceccon (University of Bolzano, Italy) and William Hobbs (University of Leeds, U.K.) for preparation of methyl-labeled Malate Synthase G and ΔST-DNAJB6B samples, respectively, and Drs. James Baber, Dan Garrett, and Jinfa Ying (NIDDK, NIH) for technical support. This work was supported by the Intramural Program of the National Institute of Diabetes and Digestive and Kidney Diseases, National Institutes of Health (DK-029023 to G.M.C.).

REFERENCES

(1) Palmer, A. G.; Williams, J.; McDermott, A. Nuclear Magnetic Resonance Studies of Biopolymer Dynamics. *J. Phys. Chem.* **1996**, *100*, 13293−13310.

(2) Mittermaier, A. K.; Kay, L. E. New Tools Provide New Insights in NMR Studies of Protein Dynamics. *Science* **2006**, *312*, 224−228.

(3) Palmer, A. G. Chemical Exchange in Biomacromolecules: Past, Present, and Future. *J. Magn. Reson.* **2014**, *241*, 3−17.

(4) Zhuravleva, A.; Korzhnev, D. M. Protein Folding by NMR. *Prog. Nucl. Magn. Reson. Spectrosc.* **2017**, *100*, 52−77.

(5) Carr, H. Y.; Purcell, E. M. Effects of Diffusion on Free Precession in Nuclear Magnetic Resonance Experiments. *Phys. Rev.* **1954**, *94*, 630−638.

(6) Meiboom, S.; Gill, D. Modified Spin-Echo Method for Measuring Nuclear Relaxation Times. *Rev. Sci. Instrum.* **1958**, *29*, 688−691.

(7) Palmer, A. G.; Kroenke, C. D.; Loria, J. P. NMR Methods for Quantifying Microsecond-to-Millisecond Motions in Biological Macromolecules. *Methods Enzymol.* **2001**, *339*, 204−238.

(8) Palmer, A. G.; Grey, M. J.; Wang, C. Solution NMR Spin Relaxation Methods for Characterizing Chemical Exchange in High-Molecular-Weight Systems. *Methods Enzymol.* **2005**, *394*, 430−465.

(9) Korzhnev, D. M.; Kay, L. E. Probing Invisible, Low-Populated States of Protein Molecules by Relaxation Dispersion NMR Spectroscopy: An Application to Protein Folding. *Acc. Chem. Res.* **2008**, *41*, 442−451.

(10) Rosenzweig, R.; Kay, L. E. Bringing Dynamic Molecular Machines into Focus by Methyl-TROSY NMR. *Annu. Rev. Biochem.* **2014**, *83*, 291−315.

(11) Tugarinov, V.; Kay, L. E. Methyl Groups as Probes of Structure and Dynamics in NMR Studies of High-Molecular-Weight Proteins. *Chembiochem* **2005**, *6*, 1567−1577.

(12) Sheppard, D.; Sprangers, R.; Tugarinov, V. Experimental Approaches for NMR Studies of Side-chain Dynamics in High-Molecular-Weight Proteins. *Prog. Nucl. Magn. Reson. Spectrosc.* **2010**, *56*, 1−45.

(13) Tugarinov, V.; Kay, L. E. Separating Degenerate ^{1}H Transitions in Methyl Group Probes for Single-Quantum ^{1}H-CPMG Relaxation Dispersion NMR Spectroscopy. *J. Am. Chem. Soc.* **2007**, *129*, 9514−9521.

(14) Yuwen, T.; Huang, R.; Vallurupalli, P.; Kay, L. E. A Methyl-TROSY-Based ^{1}H Relaxation Dispersion Experiment for Studies of Conformational Exchange in High Molecular Weight Proteins. *Angew. Chem., Int. Ed. Engl.* **2019**, *58*, 6250−6254.

(15) Tugarinov, V.; Karamanos, T. K.; Ceccon, A.; Clore, G. M. Optimized NMR Experiments for the Isolation of $I = 1/2$ Manifold Transitions in Methyl Groups of Proteins. *ChemPhysChem* **2020**, *21*, 13−19.

(16) Korzhnev, D. M.; Mittermaier, A. K.; Kay, L. E. Cross-Correlated Spin Relaxation Effects in Methyl ^{1}H CPMG-Based Relaxation Dispersion Experiments: Complications and a Simple Solution. *J. Biomol. NMR* **2005**, *31*, 337−342.

(17) Baldwin, A. J.; Religa, T. L.; Hansen, D. F.; Bouvignies, G.; Kay, L. E. $^{13}CHD_2$ Methyl Group Probes of Millisecond Time Scale Exchange in Proteins by ^{1}H Relaxation Dispersion: An Application to Proteasome Gating Residue Dynamics. *J. Am. Chem. Soc.* **2010**, *132*, 10992−10995.

(18) Tugarinov, V.; Hwang, P. M.; Ollerenshaw, J. E.; Kay, L. E. Cross-Correlated Relaxation Enhanced ^{1}H-^{13}C NMR Spectroscopy of Methyl Groups in Very High Molecular Weight Proteins and Protein Complexes. *J. Am. Chem. Soc.* **2003**, *125*, 10420−10428.

(19) Mueller, L. Sensitivity Enhanced Detection of Weak Nuclei Using Heteronuclear Multiple Quantum Coherence. *J. Am. Chem. Soc.* **1979**, *101*, 4481−4484.

(20) Bax, A.; Griffey, R. H.; Hawkins, B. L. Correlation of Proton and Nitrogen-15 Chemical Shifts by Multiple Quantum NMR. *J. Magn. Reson.* **1983**, *55*, 301−315.

(21) Korzhnev, D. M.; Kloiber, K.; Kanelis, V.; Tugarinov, V.; Kay, L. E. Probing Slow Dynamics in High Molecular Weight Proteins by Methyl-TROSY NMR Spectroscopy: Application to a 723-Residue Enzyme. *J. Am. Chem. Soc.* **2004**, *126*, 3964−3973.

(22) Shaka, A. J.; Keeler, J.; Frenkiel, T.; Freeman, R. An Improved Sequence for Broadband Decoupling: Waltz-16. *J. Magn. Reson.* **1983**, *52*, 335−338.

(23) Marion, D.; Ikura, M.; Tschudin, R.; Bax, A. Rapid Recording of 2D NMR Spectra without Phase Cycling. Application to the Study of Hydrogen Exchange in Proteins. *J. Magn. Reson.* **1989**, *85*, 393−399.

(24) Neudecker, P.; Robustelli, P.; Cavalli, A.; Walsh, P.; Lundström, P.; Zarrine-Afsar, A.; Sharpe, S.; Vendruscolo, M.; Kay, L. E. Structure of an Intermediate State in Protein Folding and Aggregation. *Science* **2012**, *336*, 362−366.

(25) Neudecker, P.; Zarrine-Afsar, A.; Choy, W. Y.; Muhandiram, D. R.; Davidson, A. R.; Kay, L. E. Identification of a Collapsed Intermediate with Non-Native Long-Range Interactions on the Folding Pathway of a Pair of Fyn SH3 Domain Mutants by NMR Relaxation Dispersion Spectroscopy. *J. Mol. Biol.* **2006**, *363*, 958−976.

(26) Libich, D. S.; Tugarinov, V.; Clore, G. M. Intrinsic Unfoldase/Foldase Activity of the Chaperonin Groel Directly Demonstrated Using Multinuclear Relaxation-Based NMR. *Proc. Natl. Acad. Sci. U.S.A.* **2015**, *112*, 8817−8823.
(27) Tugarinov, V.; Clore, G. M. The Measurement of Relaxation Rates of Degenerate ^{1}H Transitions in Methyl Groups of Proteins Using Acute Angle Radiofrequency Pulses. *J. Magn. Reson.* **2021**, *330*, 107034.
(28) Karamanos, T. K.; Tugarinov, V.; Clore, G. M. Unraveling the Structure and Dynamics of the Human Dnajb6b Chaperone by NMR Reveals Insights into Hsp40-Mediated Proteostasis. *Proc. Natl. Acad. Sci. U.S.A.* **2019**, *116*, 21529−21538.
(29) Tugarinov, V.; Karamanos, T. K.; Clore, G. M. Optimized Selection of Slow-Relaxing ^{13}C Transitions in Methyl Groups of Proteins: Application to Relaxation Dispersion. *J. Biomol. NMR* **2020**, *74*, 673−680.
(30) Aguilar, J. A.; Nilsson, M.; Bodenhausen, G.; Morris, G. A. Spin Echo NMR Spectra without J Modulation. *Chem. Commun. (Camb)* **2012**, *48*, 811−813.
(31) Kiraly, P.; Dal Poggetto, G.; Castañar, L.; Nilsson, M.; Deák, A.; Morris, G. A. Broadband Measurement of True Transverse Relaxation Rates in Systems with Coupled Protons: Application to the Study of Conformational Exchange. *Chem. Sci.* **2021**, *12*, 11538−11547.
(32) Takegoshi, K.; Ogura, K.; Hikichi, K. A Perfect Spin Echo in a Weakly Homonuclear J-Coupled Two Spin-System. *J. Magn. Reson.* **1989**, *84*, 611−615.
(33) Torres, A. M.; Zheng, G.; Price, W. S. J-Compensated PGSE: An Improved NMR Diffusion Experiment with Fewer Phase Distortions. *Magn. Reson. Chem.* **2010**, *48*, 129−133.

https://doi.org/10.1021/acs.jpclett.2c02937
J. Phys. Chem. Lett. 2022, 13, 11271−11279